





# Electronic and optical properties of a $D_2^+$ complex in two-dimensional quantum dots with Gaussian confinement potential

H. Sari<sup>1</sup> , E. B. Al<sup>2</sup>, E. Kasapoglu<sup>2</sup>, S. Sakiroglu<sup>3</sup>, I. Sökmen<sup>3,4</sup>, M. Toro-Escobar<sup>5</sup>, C. A. Duque<sup>5,a</sup> 

<sup>1</sup> Department of Mathematics and Natural Science Education, Faculty of Education, Sivas Cumhuriyet University, 58140 Sivas, Turkey

<sup>2</sup> Department of Physics, Faculty of Science, Sivas Cumhuriyet University, 58140 Sivas, Turkey

<sup>3</sup> Physics Department, Faculty of Science, Dokuz Eylül University, 35390 Izmir, Turkey

<sup>4</sup> Dokuz Eylül University, Izmir, Turkey

<sup>5</sup> Grupo de Materia Condensada-UdeA, Instituto de Física, Facultad de Ciencias Exactas y Naturales, Universidad de Antioquia UdeA, Calle 70 No. 52-21 Medellín, Colombia

Received: 6 January 2022 / Accepted: 24 March 2022

© The Author(s), under exclusive licence to Società Italiana di Fisica and Springer-Verlag GmbH Germany, part of Springer Nature 2022

**Abstract** Using the two-dimensional diagonalization method and the effective mass approximation, the electronic structure and intersubband optical absorption of the singly ionized double donor complex confined in a Gaussian quantum dot have been investigated. The obtained results indicated that the quantum dot size and internuclear distance significantly affect the binding energy, dissociation energy, equilibrium distance, and amplitude of the optical absorption. Also, we conclude that a significant increase in the amplitude of the dipole-related matrix element and the energy difference between the two lowest-lying energy states is observed when the distance between the donor atoms is in the order of the quantum dot size. Consequently, the electronic and optical properties can be precisely tuned by controlling the system's size and the internuclear distance.

## 1 Introduction

Motivation towards the possibilities of realization of new high-technology electronic devices based on a two-level system has brought about remarkable interest over the past decades [1]. Quantum dots (QDs), which are zero-dimensional nanostructures, stand as promising candidates for applications in energy conversion, medical imaging, and very recently in quantum communication [2, 3]. On account of the discrete nature of energy levels due to the three-dimensional spatial confinement of the charge carriers, QDs exhibit unique electronic and optical properties substantially different from their bulk counterparts [4, 5]. Intensive theoretical and experimental researches revealed the crucial impact of the size/shape of the structure, the number/type of confined charge carriers and the effects of external fields on the electronic, optical, and transport properties of QDs [6–16]. Rezaei and Kish have used the direct matrix diagonalization method for the calculation of binding energy of a hydrogenic donor impurity in a two-dimensional QD (2DQD) considering simultaneous effects of electric and magnetic fields, hydrostatic pressure, and temperature [17]. The behavior of the magnetic field-related binding energy of a hydrogenic impurity in a spherical QD has been investigated by Xiao and coworkers [18]. The electron energy spectrum and optical absorption coefficients (OACs) in a parabolic disk-like QD with Gaussian impurity in the presence of Rashba spin-orbit interaction and static magnetic field have been presented by Hosseinpour et al. [19]. The ground state binding energy of a hydrogenic donor impurity in a vertically coupled, cylindrical-shaped multiple GaAs QD structure under the influence of hydrostatic pressure and electric field has been studied by Duque et al. [20]. Generally, in theoretical calculations, rectangular well, spherical and parabolic potentials are utilized for modeling of confining potential [21, 22]. Nevertheless, Gaussian potential can be a more appropriate and realistic model potential for describing electronic excitations, ionization, and tunneling processes in QDs due to its essential advantages (finite depth, range, and continuity at the dot boundary) [23–27]. The Gaussian potential has already been used by researchers to study various properties of QDs. For instance, A. Boda has calculated the electronic and optical properties of a single electron Gaussian GaAs QD considering the presence of electric, magnetic, and Aharonov–Bohm flux field [24]. The binding energies for hydrogenic-like donor impurity in three- and two-dimensional QDs defined by Gaussian confining potential have been studied in Ref. [25]. Research conducted on the electronic and magnetic properties of a two-electron Gaussian QD with spin-Zeeman term exhibits the remarkable dependence on dot size, magnetic field, and electron–electron interaction [27]. A detailed study of Gaussian QDs considering exciton states, transition frequency of strong-coupling polaron, and exchange interaction has been reported in Refs. [28–31]. Calculations included diagonalization procedures by using, for example, translational invariant harmonic product states.

I. Sökmen, Dokuz Eylül University, Retired.

<sup>a</sup> e-mail: [carlos.duque1@udea.edu.co](mailto:carlos.duque1@udea.edu.co) (corresponding author)

On the other hand, advances in the growth and characterization techniques in material science have promoted studies related to the explorations of physical properties of QDs with singly ionized double donor system ( $D_2^+$ ) [32–34]. This artificial molecular system consists of two positive charge centers where one of the two excess electrons is ionized. Intriguing molecular features and its possibility for implementation as a charge qubit in semiconductors make it worth studying [35]. Kang and coworkers investigated the energy levels of the ground, and first excited states of spherical QDs with  $H_2^+$ -like impurities and feasibility of their usage as a charge qubits [35,36]. Influences of spatial and dielectric confinement modulations on energy splittings, spontaneous emission rates, and charge density distributions of a  $D_2^+$  artificial molecule in a spherical QD have been reported by Movilla et al. [37]. Results of their research exhibit the possible tunability of tunnel coupling strength and charge-density distribution of the system with an appropriate choice of dot size and medium. Analysis of the lowest-lying molecular states of a singly ionized on-axis double-donor system considered in an axially symmetric and vertically coupled QDs under the influence of magnetic field has been carried out in Ref. [38]. The authors discuss the dot morphology- and field-dependent variations in the energies and electronic density of states obtained via numerical calculations. Recently Hernandez et al. [4] have carried out a detailed work on the magnetic field induced OACs of a  $D_2^+$  singly ionized double donor system confined in a quantum ring. Obtained results show that the optical response of the system is strongly dependent on the position and angle formed by the double-donor system, external magnetic field, hydrostatic pressure, and sample temperature.

Although several works examining the  $D_2^+$ -related structural properties of QDs, to the best of our knowledge, there have been no reports on the electronic structure and optical response of a singly ionized double-donor system in a Gaussian quantum dot. In the present study, we examine specifically the energy spectrum, binding energy, and intersubband optical absorption of a  $D_2^+$  artificial molecule confined in QD with Gaussian potential. The organization of the paper is as follows: Sect. 2 contains the theoretical description; the obtained results are discussed in Sect. 3 and finally, the conclusions are given in Sect. 4.

## 2 Theoretical model

In this study, our aim is to calculate the energy states and optical sensitivity of a single ionized double donor complex  $D_2^+$  formed by combining a conduction band electron and two donor centers in a 2DQD. Within the framework of the effective mass approximation, the two-dimensional time-independent Schrödinger equation for the  $D_2^+$  artificial molecular complex located in the 2DQD is given by

$$\left[ -\frac{\hbar^2}{2m^*} \left( \frac{\partial^2}{\partial x^2} + \frac{\partial^2}{\partial y^2} \right) + V(x, y) + V_C(x, y) + V_{D_1D_2} \right] \psi(x, y) = E \psi(x, y), \quad (1)$$

where  $m^*$  is the electron effective mass,  $V(x, y)$  is the  $xy$ -plane Gaussian confinement potential,  $V_C(x, y)$  is the attractive Coulomb interaction potential between the electron and donor atoms and  $V_{D_1D_2}$  is the donor–donor repulsive Coulomb potential. The Gaussian electron confining potential is given by

$$V(x, y) = V_0 \left( 1 - e^{-(x^2+y^2)/R^2} \right), \quad (2)$$

where  $R$  is the characteristic confinement length defined as the effective radius of the 2DQD. The vector position of the first and second impurity atom is given as  $\mathbf{r}_{D_1} = x_1 \hat{x} + y_1 \hat{y}$  and  $\mathbf{r}_{D_2} = x_2 \hat{x} + y_2 \hat{y}$ , respectively. The attractive Coulomb interaction potential between the electron and donor atoms takes the form

$$V_C(x, y) = - \sum_{i=1}^2 \frac{e^2}{4\pi\epsilon\epsilon_0 \sqrt{(x-x_i)^2 + (y-y_i)^2}}, \quad (3)$$

whereas the donor–donor repulsive Coulomb potential is written as:

$$V_{D_1D_2} = \frac{e^2}{4\pi\epsilon\epsilon_0 \sqrt{(x_1-x_2)^2 + (y_1-y_2)^2}}, \quad (4)$$

where  $\epsilon$  and  $\epsilon_0$  are respectively the GaAs static dielectric constant and vacuum permittivity.

In this study, both donor atoms are symmetrically placed on the  $x$ -axis, i.e.,  $y_1 = y_2 = 0$  and  $x_1 = -x_2 = D/2$ . Thus, the separation between the donor atoms defined as the internuclear distance is  $|\mathbf{r}_{D_2} - \mathbf{r}_{D_1}| = |x_2 - x_1| = 2x_1 = D$ .

Since the analytical solution of the eigenvalue equation given in Eq. (1) is not possible, the bound electron energy levels and the corresponding eigenfunctions are obtained using the two-dimensional diagonalization technique [39–42]. Also, the energies and wave functions corresponding to the Eq. (1) are calculated with the *COMSOL-Multiphysics* [43] software, which uses a FEM to solve the partial differential equation numerically. A complete description of the *COMSOL-Multiphysics* licensed software can be found in [44,45]. Since the wavefunction is finite, the Dirichlet boundary condition implies that any of its values far away are equal to zero. For layered structures such as the one in the current study, the Schrödinger equation interface accounts for the discontinuity in the effective mass by implementing the BenDaniel-Duke boundary conditions [46–49].

At this stage of the manuscript, it is important to clarify the advantages and disadvantages of the diagonalization method used to solve the Schrödinger equation. The diagonalization methods are typically used to determine the low-lying eigenvalues and eigenfunctions of analytically unsolvable quantum systems with finite dimensions. Although methods are limited to small lattice sizes, they have become increasingly popular over the past few decades [50–53]. By means of this method, the energy spectrum can also be easily obtained under externally applied fields, regardless of the form of the confinement potential of the quantum system. The main disadvantage of this method is that the number of basis elements must be large enough in order to calculate high-level energy levels precisely. This causes the runtime to be much longer than expected, especially in three-dimensional quantum systems.

After the energies and corresponding wave functions are obtained, the linear, third order nonlinear, and total OACs for intersubband transitions in 2DQD are calculated using the iteration approach in compact density matrix formalism [54–56]. To calculate the OACs of the material due to intersubband transitions, we assume that the system is excited by an external electromagnetic wave with frequency- $\omega$  and polarized in the  $x$ -direction. The time dependent electric field vector of this optical wave can be written as

$$\mathbf{E}(t) = 2 \mathbf{E}_0 \cos(\omega t) = \mathbf{E}_0 (e^{-i \omega t} + e^{i \omega t}). \tag{5}$$

Based on the compact density matrix method, the following expression is used for the total OAC in a two-level system approach:

$$\alpha(\omega, I) = \alpha^{(1)}(\omega) + \alpha^{(3)}(\omega, I), \tag{6}$$

where

$$\alpha^{(1)}(\omega) = \sqrt{\frac{\mu}{\epsilon_r}} \frac{\sigma_s \Gamma_{ij}}{(E_{ij} - \hbar \omega)^2 + (\hbar \Gamma_{ij})^2} \hbar \omega |M_{ij}|^2 \tag{7}$$

and

$$\alpha^{(3)}(\omega, I) = -\sqrt{\frac{\mu}{\epsilon_r}} \left( \frac{I}{2 n_r \epsilon_0 c} \right) \frac{\sigma_s \Gamma_{ij} \hbar \omega |M_{ij}|^2}{[(E_{ij} - \hbar \omega)^2 + (\hbar \Gamma_{ij})^2]^2} \left[ 4 |M_{ij}|^2 - \frac{|M_{jj} - M_{ii}|^2 [3 E_{ij}^2 - 4 E_{ij} \hbar \omega + \hbar^2 (\omega^2 - \Gamma_{ij}^2)]}{E_{ij}^2 + (\hbar \Gamma_{ij})^2} \right] \tag{8}$$

are the linear and third-order nonlinear OACs, respectively. In the above equations,  $\mu$  is the susceptibility of the system defined as  $\mu = 1/\epsilon_0 c^2$ , where  $c$  is the speed of light in the vacuum. In addition,  $\sigma_s$  is the electron density in the system and  $I$  is the incident optical intensity defined as  $I = 2 \epsilon_0 n_r c |\tilde{E}|^2$ . Additionally,  $\epsilon_r$  is the real part of the permittivity associated with the refractive index- $n_r$  of the material in the form  $\epsilon_r = n_r^2 \epsilon_0$ .  $M_{ij} = \langle \psi_i | e x | \psi_j \rangle$  represents the electric dipole moment matrix element, where  $\psi_i$  and  $\psi_j$  are the initial and final eigenfunctions for the optical transition,  $E_{ij} = E_j - E_i$  is the energy difference between the corresponding electronic levels, and  $\hbar \omega$  is the incident photon energy. Finally,  $\Gamma_{ij} = 1/T_{ij}$  is the relaxation rate defined during the relaxation time  $T_{ij}$ . The relaxation rate is strongly related not only to the materials that make up the QDs, but also to some other factors such as boundary conditions, temperature of the system, and collision processes associated with electron-impurity, electron-phonon, and electron-electron interactions.

### 3 Results and discussion

At this stage, we will discuss the numerical results obtained by the two-dimensional diagonalization method and FEM regarding the electronic structure, dissociating energy, and optical sensitivity of the  $D_2^+$  complex in the 2DQD with Gaussian confining potential. In the numerical calculations, we used the following physical parameters commonly used for *GaAs*-based heterostructures:  $\epsilon = 13.18$ ,  $V_0 = 228 \text{ meV}$ ,  $m^* = 0.067 m_0$  (where  $m_0$  is the mass of free electron),  $T_{ij} = 0.14 \text{ ps}$ ,  $\mu = 4 \pi \times 10^{-7} \text{ H/m}$ ,  $n_r = 3.63$ ,  $\sigma_s = 1.0 \times 10^{23} \text{ m}^{-3}$ , and  $I = 400 \text{ MW/m}^2$  [57–60].

In Fig. 1, we present the variation of the total energy of the  $D_2^+$  complex corresponding to the ground and first excited state as a function of the internuclear distance- $D$  for three different QD size values. Solid lines are obtained via a diagonalization method, whereas full symbols come from FEM calculations. The first remarkable point to emphasize in this figure is that when the impurity atoms are very close to each other, the first excited energy level degenerates doubly since the effective potential energy of the system ( $V(x, y) + V_C(x, y)$ ) is almost circularly symmetrical. As the distance between the impurity atoms increases, the symmetrical structure of the potential begins to deteriorate thus, the degeneracy observed in the first excited state disappears, and as a result, this energy state is split into two levels,  $E_2$  and  $E_3$ . Figure 2 clearly shows how the circular symmetry of the effective potential of the system is broken with increasing the internuclear distance- $D$ . It should be noted that in large-sized QDs, degeneracy in the first excited state disappears at larger values of the  $D$ -distance. Because as seen in Fig. 2, the internuclear distance dependence of the effective potential symmetry for large  $R$  values is relatively weak. Also, as seen in Fig. 1, as the effective QD size- $R$  increases, the equilibrium distance (total energy minimum) increases (decreases). This means that as the geometric confinement weakens, the kinetic energy of the electron decreases and a more stable electrostatic bonding is formed between the electron and the donor atoms.

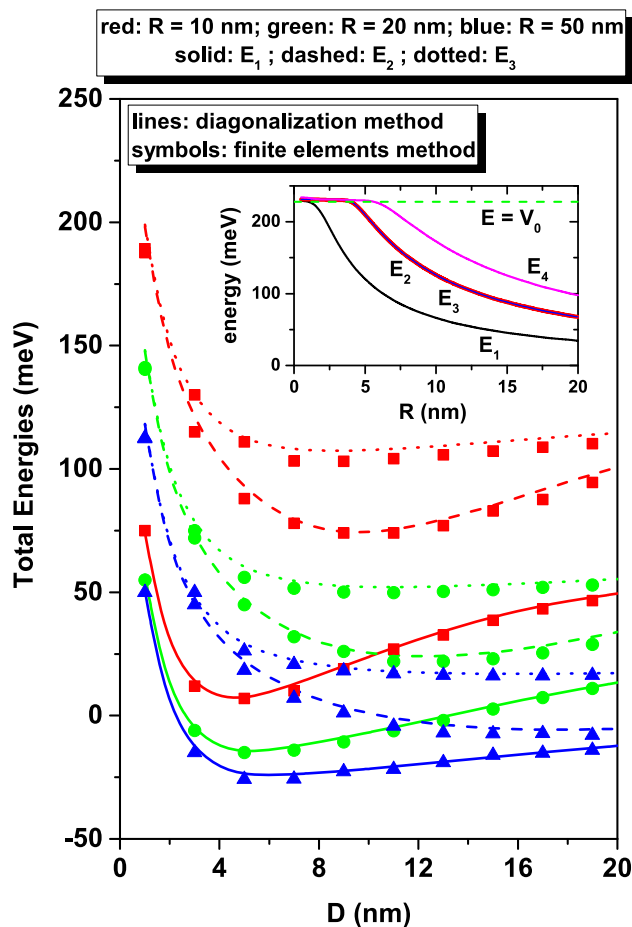


**Fig. 1** The total energy of the  $D_2^+$  complex as a function of the internuclear distance- $D$  for three different values of the effective QD radius- $R$ . The inset shows the dot radius dependence of the lowest four energy levels for a confined electron in the two-dimensional quantum dots with Gaussian confinement potential without the impurity effects

The inset in Fig. 1 shows the lowest four bound energy levels for a confined electron in the two-dimensional QD with Gaussian confinement potential and without the impurity effects. The degeneration of the first and second excited states is observed, with  $2p$ -like symmetry. In general, as the dot radius increases, the confining effect on the electron decreases, and consequently, the energy of all the states shown here decreases. In the strong confinement regime, that is, as the radius of the QD is reduced, the higher energy states begin to escape from the confinement and the number of bound states decreases. For example, for  $R = 2.5$  nm, only the ground state is confined while for  $R = 4.24$  nm the system supports three confined states, the ground state and the first two excited states, which due to the effects of circular symmetry are doubly degenerate. The horizontal dashed line corresponds to the energy associated with the potential barrier, the limit for bound and unbound states in the QD.

In order to certify our results obtained through the diagonalization method, we have decided to implement a numerical calculation through the finite element method. In Fig. 1, such results are reported with filled symbols. As can be seen, there is a complete correlation between the results obtained by the two methods. In general, the energies obtained by the FEM, when they differ from those calculated by the diagonalization method, are slightly lower with a difference of less than 2.0%. The differences come from the degree of convergence required by both methods. In the case of the energies obtained by the diagonalization method, the convergence was imposed up to 2.0 meV for the first three bound states, while in the case of the EMF, a convergence of 0.01 meV was imposed. The technical details of the FEM calculations are: mesh: triangular; mesh vertices: 13633; triangles: 26944; edge elements: 320; vertex elements: 4; maximum element size: 1.48 nm; minimum elements size: 0.005 nm; maximum elements growth rate: 1.25; bend factor: 0.25; resolution of narrow regions: 1; minimum element quality: 0.686; element area ratio: 0.3207; and mesh area: 1131 nm<sup>2</sup>.

To understand a little more the characteristics of the total confining potential, in Fig. 3, we present the projection on the  $y = 0$  axis of the sum  $V(x, y = 0) + V_c(x, y = 0)$  for  $R = 5$  nm considering the case without impurities and three different cases of symmetric impurities positioning along the  $x$ -axis. In general, it is appreciated that the presence of localized impurities in the vicinity of the center of the QD translates into a rather deep potential that essentially preserves circular symmetry. In this case, the effects of the two impurities reinforce each other, and a significant redshift of the energy levels should be observed with a subsequent significant value of binding energy. As the  $D$ -parameter increases, the additive effect of the two impurity potentials is lost, and the bottom

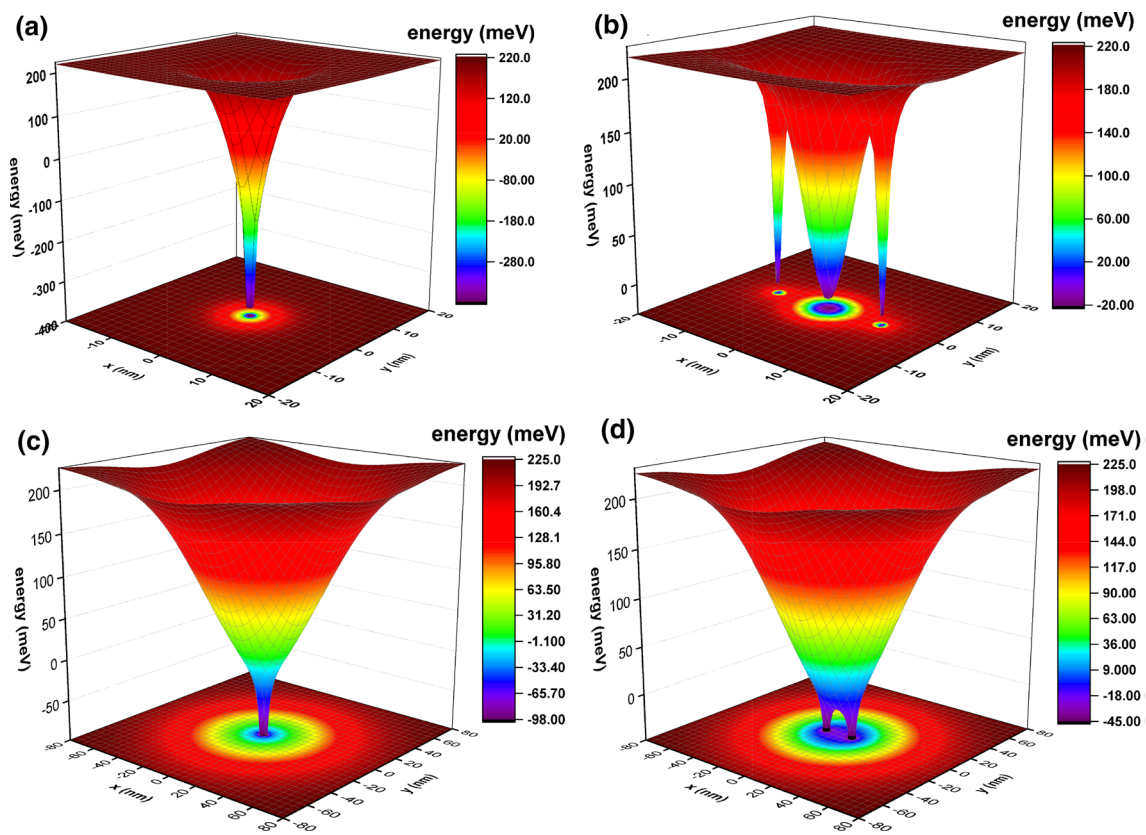


**Fig. 2** The variation of the effective potential ( $V(x, y) + V_C(x, y)$ ). Results are for  $(R, D)$  in nm units as follows: (5, 2) (a), (5, 20) (b), (50, 2) (c), (50, 20) (d)

of the potential well tends systematically to return to the zero of energy shown by the horizontal dashed raven that appears in the four panels. As the  $D$ -parameter becomes significantly large, the system behaves like a Gaussian well disturbed by two impurity potentials, in which case the electronic probability density is maximum in the central region of the QD with contributions of in two potential wells symmetrically located along the  $x$ -axis. It is clearly seen when observing Figs. 3(b,c,d) that the increase of the  $D$ -parameter translates into an effective increase in the size of the QD with which important variations in the binding energy should be observed. In the absence of impurity, the ground state exhibits  $s$ -like symmetry, and the first two excited states, which are degenerate, have  $p$ -like symmetry. There will be a  $2p_x$ -like state with its two lobes located along the  $x$ -axis ( $2p_x$ -like) and a  $2p_y$ -like state with its two lobes located along the  $y$ -axis ( $2p_y$ -like). It is clear that when moving the impurities along the  $x$  axis, such degeneration should be broken with important changes in the energy associated with the  $2p_x$ -like state since there will be moments when the impurities will be located in the regions of the lobes of said state. It is important to note that for  $R$  and  $D$  large enough, the system will behave as two independent impurities, and the ground state of the system will be doubly degenerate with two states of symmetric and antisymmetric character. Finally, we must stress that the two impurities cannot be localized at the same spatial point, and this is consistent with the divergence of the potential in Eq. (4).

In Fig. 4, we present the variation of the  $D_2^+$  binding energy corresponding to the first four energy levels as a function of the effective QD size- $R$  for three different values of the internuclear distance- $D$ . The binding energy of the  $D_2^+$  complex, which corresponds to the  $n$ -th state, is defined as the difference between the  $n$ -th state energy of the system with and without donor atoms. The last term does not include the repulsive interaction between the donor atoms since the repulsive interaction between the donor atoms does not contribute to the binding energy [32]. For all the internuclear distance values considered, a general conclusion observed here is that as the  $R$ -value increases, the binding energy increases, reaches a maximum value, and then decreases and converges to a particular value. This behavior is a general feature of the geometric confinement dependence of the Coulombic binding in hydrogen-like systems. As expected, when the distance between donor atoms is very small (on the order of atomic size), due to the almost circular symmetry of the effective confinement potential, the first excited energy level is doubly degenerate, and the binding energies corresponding to the  $E_2$  and  $E_3$  states are coincident. On the other hand, when the donor atoms are far from each other, the difference between the binding energies corresponding to the  $E_2$  and  $E_3$  states increases significantly, as the symmetrical property of the effective potential is disturbed. Also, as can be seen in Fig. 4c, for sufficiently large  $D$ -values, the sensitivity of the binding energies to the QD size is weak compared to the narrow QD case. Since when the distance between the donor atoms is large enough, the potential barrier between the two donor atoms becomes higher and wider, and thus the electron is less likely to be



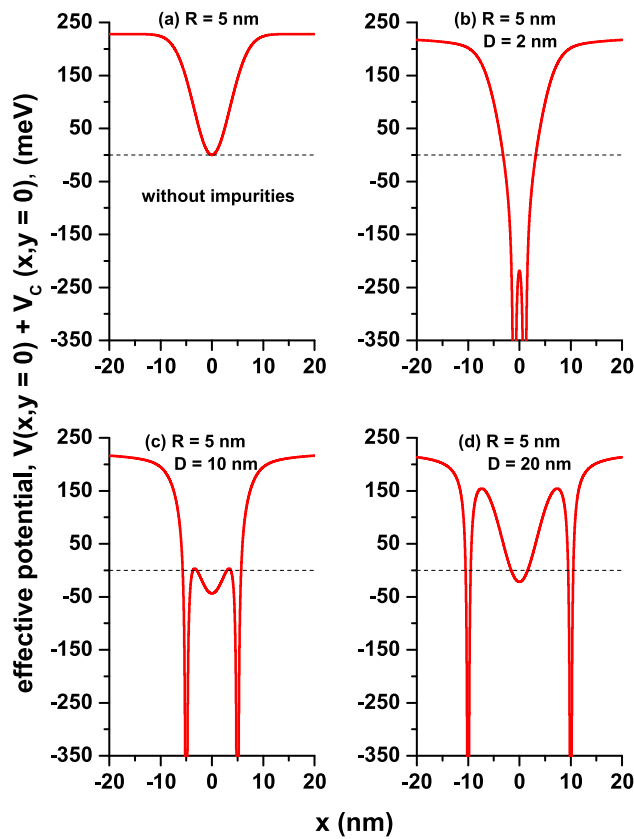


**Fig. 3** The variation of the effective potential ( $V(x, y = 0) + V_C(x, y = 0)$ ) for  $R = 5$  nm with: no impurities (a),  $D = 2$  nm (b),  $D = 10$  nm (c), and  $D = 20$  nm (d)

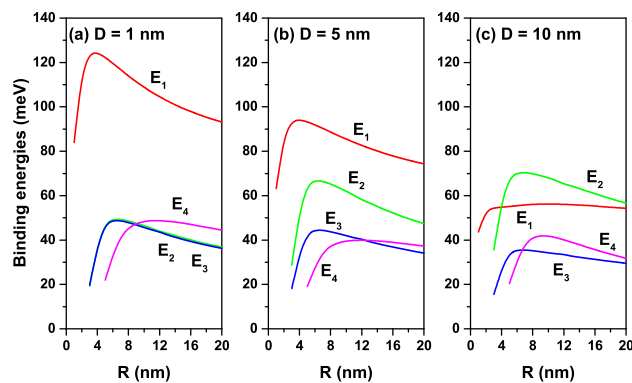


**Fig. 4** The binding energy of the  $D_2^+$  complex as a function of the effective QD radius- $R$  for different values of the internuclear distance- $D$

shared by the two donor atoms and eventually localizes in a narrow region around one of the two donor atoms. For this reason, the sensitivity of the electron to the variation of effective potential is reduced.

In Fig. 5 we show the variation of the OACs as a function of the incident photon energy for different values of the effective QD radius- $R$  and the internuclear distance- $D$ . As can be seen in Fig. 5, the quantum dot size- $R$  and internuclear distance- $D$  cause significant changes in the absorption spectrum between the states of the  $D_2^+$  molecular complex confined in a 2DQD. In the case where the QD dimension is small, if the internuclear distance is also small enough, the  $M_{12}$  matrix element amplitude also takes small values since the wave functions corresponding to the related states are localized in a narrow region of the two-dimensional space. On the other hand, when the internuclear distance is as large as the QD dimension, a significant increase in the amplitude of the  $M_{12}$  matrix element is observed as a result of the wave functions spreading over a wider area. However, when the internuclear distance reaches sufficiently large values, the Coulomb potential has a wider and higher internal barrier as mentioned above. The electron

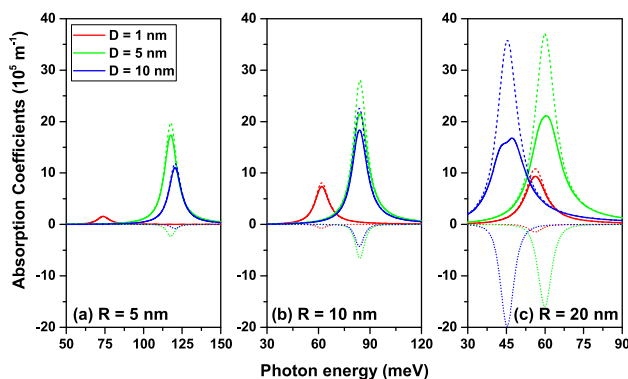


**Fig. 5** The variation of the optical absorption coefficients as a function of the incident photon energy for different values of the effective QD radius- $R$  and the internuclear distance- $D$

**Table 1** The effect of  $R$  and  $D$  parameters on the matrix element  $M_{12}$  and the energy difference  $\Delta E_{12}$

	$R$ (nm)	$\Delta E_{12}$ (meV)	$ M_{12} ^2$ (nm <sup>2</sup> )
$D = 1 \text{ nm}$	5	73.76	3.54
	10	61.72	4.64
	20	56.04	5.63
$D = 5 \text{ nm}$	5	117.52	5.24
	10	84.04	7.40
	20	59.81	10.07
$D = 10 \text{ nm}$	5	120.01	4.02
	10	83.74	6.66
	20	45.14	11.39

cannot easily transverse between donor atoms and is therefore localized in a narrow space. Thus, the amplitude of the  $M_{12}$  matrix element decreases, which leads to a decrease in the OAC peak amplitude. This feature is clearly seen in Fig. 5. In the case of larger QDs where the quantum confinement effect is weaker, the effect of internuclear distance on the absorption spectrum becomes much more pronounced since the main term for the spatial confinement of the electron is the effective Coulomb potential. The explanations we made by associating the effect of  $R$  and  $D$  parameters on the absorption spectrum with the change of the matrix elements are supported by the data in Table 1. On the other hand, according to the variation of electron energy levels depending on the  $R$  and  $D$  parameters (see Table 1), the absorption peak position for small  $R$  values shifts towards higher photon energies with increasing  $D$  values. In contrast, at large  $R$  values, in the absorption peak position, first a blue shift and then a red shift is observed. The variation of the electronic spectrum of the  $D_2^+$  complex depending on the internuclear distance and QD size parameters contributes to the evaluation of this complex as a two-level system that plays an important role in the quantum computing process.

### 4 Conclusions

We have investigated a theoretical study on the energy spectrum, binding energy, and OACs of the  $D_2^+$  complex confined in a two-dimensional Gaussian QD. We analyzed the effect of the geometric size and internuclear distance on the binding energy, equilibrium distance, and OACs of the  $D_2^+$  complex. The obtained results of the  $D_2^+$  system indicated that the QD size and internuclear distance significantly affect the binding energy, dissociation energy, equilibrium distance, and amplitude of the OACs. We conclude that a significant increase in the amplitude of the matrix element and the energy difference between the two lowest-lying energy states is observed when the distance between the donor atoms is in the order of the QD size. The change of the low-lying electronic structure of the  $D_2^+$  complex with the parameters of internuclear distance and QD size provides an additional degree of freedom to consider this complex as a two-level system, which is important in the quantum computing process.

**Acknowledgements** CAD is grateful to the Colombian Agencies: CODI-Universidad de Antioquia (Estrategia de Sostenibilidad de la Universidad de Antioquia and projects "Propiedades magneto-ópticas y óptica no lineal en superredes de Grafeno", "Estudio de propiedades ópticas en sistemas semiconductores de dimensiones nanoscópicas", and "Propiedades de transporte, espintrónicas y térmicas en el sistema molecular ZincPorfirina"), and Facultad de Ciencias Exactas y Naturales-Universidad de Antioquia (CAD exclusive dedication project 2021-2022). CAD also acknowledges the financial support

from *El Patrimonio Autónomo Fondo Nacional de Financiamiento para la Ciencia, la Tecnología y la Innovación Francisco José de Caldas* (project: CD 111580863338, CT FP80740-173-2019).

**Author contributions** The contributions of the authors are as follows: HS: proposed the problem and worked on the numerical calculations and writing of the manuscript. EBA: worked on the numerical calculations and writing of the manuscript. EK: worked on the numerical calculations, in formal analysis, and writing of the manuscript. SS: worked on the formal analysis and writing of the manuscript. IS: worked on the numerical calculations and formal analysis. MT-E: worked on the numerical calculations and writing of the manuscript. CAD: worked on the numerical calculations and writing of the manuscript.

## Declarations

**Conflict of interest** The authors do not have any financial and non-financial competing interests statement.

**Data Availability Statement** This manuscript has associated data in a data repository. [Authors' comment: All the files with tables, figures, and codes are available. The corresponding author will provide all the files in case they are requested.]

## References

1. W. Gutierrez, L.F. Garcia, I.D. Mikhailov, Coupled donors in quantum ring in a threading magnetic field. *Physica E* **43**, 559–566 (2010)
2. Y. Huang, H. Zang, J.-S. Chen, E.A. Sutter, P.W. Sutter, C.-Y. Nam, M. Cotlet, Hybrid quantum dot-tin disulfide field-effect. *Appl. Phys. Lett.* **108**, 123502 (2016)
3. N. Hildebrandt, C.M. Spillmann, W. Russ Algar, T. Pons, M.H. Stewart, E. Oh, K. Susumu, S.A. Díaz, J.B. Delehanty, I.L. Medintz, Energy transfer with semiconductor quantum dot bioconjugates: a versatile platform for biosensing, energy harvesting, and other developing applications. *Chem. Rev.* **117**, 536–711 (2017)
4. N. Hernandez, R. Lopez, J.A. Alvarez, J.H. Marin, M.R. Fulla, H. Tobon, Optical absorption computation of a  $D_2^+$  artificial molecule in GaAs/Ga<sub>1-x</sub>Al<sub>x</sub>As nanometer-scale rings. *Optik* **245**, 167637 (2021)
5. D. Ghosh, S.A. Ivanov, S. Tretiak, Structural dynamics and electronic properties of semiconductor quantum dots: computational insights. *Chem. Mater.* **33**, 7848–7857 (2021)
6. D. Bejan, Impurity-related nonlinear optical rectification in double quantum dot under electric field. *Phys. Lett. A* **380**, 3836–3842 (2016)
7. A. Boda, Effect of magnetic field on the energy spectrum, binding energy and magnetic susceptibility of an impurity in a 2D Gaussian quantum dot. *Ecs J. Sol. State Sci. Techn.* **10**, 041001 (2021)
8. P. Saini, A. Chatterjee, Confinement shape effect on D-0 impurity in a GaAs quantum dot with spin-orbit coupling in a magnetic field. *Superlatt. Microstr.* **146**, 106641 (2020)
9. O. Akankan, I. Erdogan, A.I. Mese, E. Cicek, H. Akbas, The effects of geometrical shape and impurity position on the self-polarization of a donor impurity in an infinite GaAs/AlAs tetragonal quantum dot. *Ind. J. Phys.* **95**, 1341–1344 (2020)
10. S. Pal, M. Ghosh, C.A. Duque, Impurity related optical properties in tuned quantum dot/ring systems. *Phil. Mag.* **99**, 2457–2486 (2019)
11. X.F. Bai, Y.W. Zhao, H.W. Yin, Influence of hydrogen-like impurity and thickness effect on quantum transition of a two-level system in an asymmetric Gaussian potential quantum dot. *Acta Phys. Sinica* **67**, 177801 (2018)
12. M. Solaimani, Binding energy and diamagnetic susceptibility of donor impurities in quantum dots with different geometries and potentials. *Mat. Sci. Eng. B* **262**, 114694 (2020)
13. H. Bahramiyan, Electric field and impurity effect on nonlinear optical rectification of a double cone like quantum dot. *Opt. Mater.* **75**, 187–195 (2018)
14. E.C. Niculescu, C. Stan, M. Cristea, C. Trusca, Magnetic-field dependence of the impurity states in a dome-shaped quantum dot. *Chem. Phys.* **493**, 32–41 (2017)
15. A.L. Vartanian, A.L. Asatryan, L.A. Vardanyan, Influence of image charge effect on impurity-related optical absorption coefficients and refractive index changes in a spherical quantum dot. *Superlatt. Microstr.* **103**, 205–212 (2017)
16. D.S. Acosta Coden, R.H. Romero, A. Ferron, S.S. Gomez, Optimal control of a charge qubit in a double quantum dot with a Coulomb impurity. *Physica E* **86**, 36–43 (2017)
17. G. Rezaei, S. Shojaei Kish, Effects of external electric and magnetic fields, hydrostatic pressure and temperature on the binding energy of a hydrogenic impurity confined in a two-dimensional quantum dot. *Physica E* **45**, 56–60 (2012)
18. Z. Xiao, J. Zhu, F. He, Magnetic field dependence of the binding energy of a hydrogenic impurity in a spherical quantum dot. *J. Appl. Phys.* **79**, 9181 (1996)
19. P. Hosseinpour, A. Soltani-Vala, J. Barvestani, Effect of impurity on the absorption of a parabolic quantum dot with including Rashba spin-orbit interaction. *Physica E* **80**, 48–52 (2016)
20. C.M. Duque, M.G. Barseghyan, C.A. Duque, Hydrogenic impurity binding energy in vertically coupled Ga<sub>1-x</sub>Al<sub>x</sub>As quantum-dots under hydrostatic pressure and applied electric field. *Physica B* **404**, 5177–5180 (2009)
21. C. Heyn, C.A. Duque, Donor impurity related optical and electronic properties of cylindrical GaAs/Ga<sub>1-x</sub>Al<sub>x</sub>As quantum dots under tilted electric and magnetic fields. *Sci. Rep.* **10**, 9155 (2020)
22. L. Belamkadem, O. Mommadi, J.A. Vinasco, D. Laroze, A. El Moussaouy, M. Chnafi, C.A. Duque, Electronic properties and hydrogenic impurity binding energy of a new variant quantum dot. *Physica E* **129**, 114642 (2021)
23. H. Sari, E. Kasapoglu, S. Sakiroglu, I. Sokmen, C.A. Duque, Impurity-related optical response in a 2D and 3D quantum dot with Gaussian confinement under intense laser field. *Phil. Mag.* **100**, 619–641 (2020)
24. A. Boda, Intersubband optical absorption in Gaussian GaAs quantum dot in the presence of magnetic, electrical and AB flux fields. *Physica B* **575**, 411699 (2019)
25. I. Al-Hayek, A.S. Sandouqa, Energy and binding energy of donor impurity in quantum dot with Gaussian confinement. *Superlatt. Microstr.* **85**, 216–225 (2015)
26. J. Adamowski, M. Sobkowicz, B. Szafran, S. Bednarek, Electron pair in a Gaussian confining potential. *Phys. Rev. B* **62**, 4234–4237 (2000)
27. H.K. Sharma, A. Boda, B. Boyacioglu, A. Chatterjee, Electronic and magnetic properties of a two-electron Gaussian GaAs quantum dot with spin-Zeeman term: a study by numerical diagonalization. *J. Magn. Magn. Mater.* **469**, 171–177 (2019)
28. A. Gharaati, R. Khordad, A new confinement potential in spherical quantum dots: modified Gaussian potential. *Superlatt. Microstr.* **48**, 276–287 (2010)
29. R. Khordad, Use of modified Gaussian potential to study an exciton in a spherical quantum dot. *Superlatt. Microstr.* **54**, 7–15 (2013)



30. R. Khordad, Energy levels and transition frequency of strong-coupling polaron in a Gaussian quantum dot. *Mod. Phys. Lett. B* **28**, 1450153 (2014)
31. R. Khordad, Calculation of exchange interaction for modified Gaussian coupled quantum dots. *Indian J. Phys.* **91**, 869 (pp5) (2017)
32. F.J. Betancur, I.D. Mikhailov, J.H. Marinz, L.E. Oliveira, Electronic structure of donor-impurity complexes in GaAs/Ga<sub>1-x</sub>Al<sub>x</sub>As quantum wells. *J. Phys. Condens. Matter* **10**, 7283–7292 (1998)
33. R. Manjarres-Garcia, G.E. Escorcía-Salas, J. Manjarres-Torres, I.D. Mikhailov, J. Sierra-Ortega, Double-donor complex in vertically coupled quantum dots in a threading magnetic field. *Nanoscale Res. Lett.* **7**, 531 (2012)
34. M. R-Fulla, J.H. Marín, W. Gutiérrez, M.E. Mora-Ramos, C.A. Duque, Magnetic field and hydrostatic pressure. Essential properties of a  $D_2^+$  molecular complex confined in ring-like nanostructures under external probes. *Superlatt. Microstruct.* **67**, 207–220 (2014)
35. S. Kang, Y.-M. Liu, T.-Y. Shi,  $H_2^+$ -like impurities confined by spherical quantum dots: a candidate for charge qubits. *Commun. Theor. Phys.* **50**, 767–770 (2008)
36. S. Kang, Y.-M. Liu, T.-Y. Shi, The characteristics for  $H_2^+$ -like impurities confined by spherical quantum dots. *Eur. Phys. J. B* **63**, 37–42 (2008)
37. J.L. Movilla, A. Ballester, J. Planelles, Coupled donors in quantum dots: quantum size and dielectric mismatch effects. *Phys. Rev. B* **79**, 195319 (2009)
38. R. Manjarres-Garcia, G.E. Escorcía-Salas, I.D. Mikhailov, J. Sierra-Ortega, Singly ionized double donor complex in vertically coupled quantum dots. *Nanoscale Res. Lett.* **7**, 489 (2012)
39. A. Tiutiunnyk, V. Tulupenko, M.E. Mora-Ramos, E. Kasapoglu, F. Ungan, H. Sari, I. Sokmen, C.A. Duque, Electron-related optical responses in triangular quantum dots. *Physica E* **60**, 127–132 (2014)
40. A. Tiutiunnyk, V. Akimov, V. Tulupenko, M.E. Mora-Ramos, E. Kasapoglu, F. Ungan, I. Sokmen, A.L. Morales, C.A. Duque, Electronic structure and optical properties of triangular GaAs/AlGaAs quantum dots: exciton and impurity states. *Physica B* **484**, 95–108 (2016)
41. A. Tiutiunnyk, V. Tulupenko, V. Akimov, R. Demedyuk, A.L. Morales, M.E. Mora-Ramos, A. Radu, C.A. Duque, Study of electron-related intersubband optical properties in three coupled quantum wells wires with triangular transversal section. *Superlattices Microstruct.* **87**, 131–136 (2015)
42. A. Tiutiunnyk, V. Akimov, V. Tulupenko, M.E. Mora-Ramos, E. Kasapoglu, A.L. Morales, C.A. Duque, Electron and donor-impurity-related Raman scattering and Raman gain in triangular quantum dots under an applied electric field. *Eur. Phys. J. B* **89**, 107 (pp9) (2016)
43. COMSOL Multiphysics, v. 5.4. COMSOL AB, Stockholm, Sweden
44. COMSOL Multiphysics Reference Guide, Stockholm, Sweden (May 2012)
45. COMSOL Multiphysics Users Guide, Stockholm, Sweden (May 2012)
46. J.A. Vinasco, A. Radu, C.A. Duque, Propiedades electrónicas de un anillo cuántico elíptico con sección transversal rectangular. *Revista EIA* **16**, 77–87 (2019)
47. J.A. Vinasco, A. Radu, E. Kasapoglu, R.L. Restrepo, A.L. Morales, E. Feddi, M.E. Mora-Ramos, C.A. Duque, Effects of geometry on the electronic properties of semiconductor elliptical quantum rings. *Sci. Rep.* **8**, 13299 (pp15) (2018)
48. J.A. Vinasco, A. Radu, E. Niculescu, M.E. Mora-Ramos, E. Feddi, V. Tulupenko, R.L. Restrepo, E. Kasapoglu, A.L. Morales, C.A. Duque, Electronic states in GaAs-(Al, Ga)As eccentric quantum rings under nonresonant intense laser and magnetic fields. *Sci. Rep.* **9**, 1427 (pp17) (2019)
49. J.A. Vinasco, A. Radu, R.L. Restrepo, A.L. Morales, M.E. Mora-Ramos, C.A. Duque, Magnetic field effects on intraband transitions in elliptically polarized laser-dressed quantum rings. *Opt. Mater.* **91**, 309–320 (2019)
50. H.Q. Lin, J.E. Gubernatis, H. Gould, J. Tobochnik, Exact diagonalization methods for quantum systems. *Comput. Phys.* **7**, 400 (1993)
51. Constantine Yannouleas, Uzi Landman, Two-dimensional quantum dots in high magnetic fields: rotating-electron-molecule versus composite-fermion approach. *Phys. Rev. B* **68**, 035326 (pp11) (2003)
52. A. Radu, A.A. Kirakosyan, D. Laroze, H.M. Baghramyan, M.G. Barseghyan, Electronic and intraband optical properties of single quantum rings under intense laser field radiation. *J. Appl. Phys.* **116**, 093101 (pp6) (2014)
53. D. Laroze, M. Barseghyan, A. Radu, A.A. Kirakosyan, Laser driven impurity states in two-dimensional quantum dots and quantum rings. *Physica B* **501**, 1–4 (2016)
54. R. Khordad, The effect of Rashba spin-orbit interaction on electronic and optical properties of a double ring-shaped quantum dot. *Superlattice. Microst.* **110**, 146–154 (2017)
55. B. Çakir, Y. Yakar, A. Özmen, Linear and nonlinear absorption coefficients of spherical quantum dot inside external magnetic field. *Physica B* **510**, 86–91 (2017)
56. R. Khordad, Optical properties of wedge-shaped quantum dots under Rashba spin-orbit interaction. *Int. J. Mod. Phys. B* **31**, 1750055 (2017)
57. Wenfang Xie, A study of an exciton in a quantum dot with Woods-Saxon potential. *Superlatt. Microstr.* **46**, 693–699 (2009)
58. R. Khordad, Use of modified Gaussian potential to study an exciton in a spherical quantum dot. *Superlatt. Microstr.* **54**, 7–15 (2013)
59. H. Dakhlaoui, J.A. Vinasco, C.A. Duque, External fields controlling the linear and nonlinear optical properties of quantum cascade laser based on staircase-like quantum wells. *Superlatt. Microstr.* **155**, 106885 (2021)
60. E. Kasapoglu, C.A. Duque, The effects of external fields on double GaAs/AlGaAs quantum well with Manning potential. *Mater. Sci. Semicond. Process.* **137**, 106232 (pp9) (2022)